NASA Technical Memorandum 100480

The Effects of Aeroelastic Deformation on the Unaugmented Stopped-Rotor Dynamics of an X-Wing Aircraft

Michael G. Gilbert and Walter A. Silva

JUNE 1987

National Aeronautics and Space Administration

Langley Research Center
Hampton, Virginia 23665

THE EFFECTS OF AEROELASTIC DEFORMATION ON THE UNAUGMENTED STOPPED-ROTOR DYNAMICS OF AN X-WING AIRCRAFT

Michael G. Gilbert*
NASA Langley Research Center, Hampton, VA.
and
Walter A. Silva**
PRC-Kentron Inc., Hampton VA.

Abstract

A new design concept in the development of vertical takeoff and landing aircraft with high forward flight speed capability is that of the X-Wing. The X-Wing is a stiff, bearingless helicopter rotor system which can be stopped in flight and the blades used as two forward-swept wings and two aft-swept wings. Because of the unusual configuration in the fixed-wing mode, there is a high potential for aeroelastic divergence or flutter and coupling of blade vibration modes with rigid-body modes. An aeroelastic stability analysis of an X-Wing configuration aircraft was undertaken to determine if these problems could exist. This paper reports on the results of dynamic stability analyses in the lateral and longitudinal directions including the vehicle rigid-body and flexible modes. A static aeroelastic analysis using the normal vibration mode equations of motion was performed to determine the cause of a loss of longitudinal static margin with increasing airspeed. This loss of static margin was found to be due to aeroelastic 'washin' of the forward-swept blades and 'washout' of the aft-swept blades moving the aircraft aerodynamic center forward of the center of gravity. This phenomenon is likely to be generic to X-Wing aircraft.

Introduction

In recent years there has been new interest in the development of vertical takeoff and landing aircraft which are capable of high speed forward flight. Two concepts currently under consideration are the tilt-rotor and X-Wing aircraft designs. Both concepts promise to deliver an aircraft with helicopter-like hover, takeoff, and landing capability with high subsonic forward flight speeds comparable to current turboprop aircraft. In the tilt-rotor design, tandem rotors are mechanically rotated between the vertical and horizontal positions for various phases of the flight. In the X-Wing concept, the rotating rotor system is stopped in flight and used as fixed wings for forward flight.

The X-Wing itself is a stiff, bearingless, four-blade helicopter rotor system which uses circulation control aerodynamic blowing to maintain and control lift on the blades and provide cyclic, collective, and higher-harmonic control inputs. The system incorporates a mechanical brake which is used to stop the rotary motion and lock the blades into position as two forward-swept and two aft-swept wings for the high speed portions of the flight, with circulation control blowing again used to avoid flow separation, minimize drag and control lift, and provide fixed-wing flight control inputs.

A flight test program to demonstrate conversion of an X-Wing rotor from rotary to fixed-wing and fixed-wing to rotary modes is currently underway. An X-Wing rotor has been built by Sikorsky Aircraft Co. and will be flown on a modified Rotor Systems Research Aircraft (RSRA) in the near future (Ref. 1). Northrop Aircraft Corporation is assisting Sikorsky in the development of the fixed-wing flight control systems and aeroelastic stability analyses. The RSRA/X-Wing aircraft configuration is shown in Figure 1.

The unusual configuration of an X-Wing aircraft in the stopped-rotor or fixed-wing mode has led to concern about the aeroelastic stability of the blades and the potential for aeroelastic interactions with the flight control systems and flight dynamics of the vehicle. As a result, detailed aeroservoelastic (ASE) analyses of the vehicle are planned and the initial state-space models describing the vehicle aeroelastic characteristics necessary for a complete ASE analysis have been developed. This paper highlights the mathematical model formulation and describes the effects of aeroelastic deformation on the flight dynamics of the vehicle.

This paper is organized in three sections. The first section describes the development of the state-space models of the vehicle longitudinal and lateral dynamics including the effects of rigid-body dynamics, flexible-vehicle deformations, unsteady aerodynamics, and deflected control surfaces. The following section gives the results of an analysis of the vehicle dynamics including aeroelastic deformations. The third section presents the results of a static aeroelastic analysis of the vehicle for the longitudinal case. This analysis was undertaken because of an analytically predicted change in the aircraft short period dynamics due to static structural deformation, and was performed using the normal mode equations of motion of the flexible vehicle.

---

* Aerospace Engineer, Aeroservoelasticity Branch, Loads and Aeroelasticity Division. Member AIAA.

** Structures Engineer, Aerospace Technologies Division. Member AIAA.

Equations of Motion

Stability analyses of flexible aircraft require the development of suitable mathematical models describing the vehicle flight dynamics, structural dynamics, aerodynamics, and control inputs. For the analysis described here, separate state-space mathematical models for the longitudinal and lateral dynamics of the X-Wing vehicle were developed using ISAC (Interaction of Structures, Aerodynamics, and Controls) computer programs (Ref. 2).

The models were developed to accurately model the aeroelastic characteristics of the vehicle and include control surface deflections, but do not include closed-loop flight control or stability augmentation systems, higher-harmonic control systems, or hub-moment-feedback systems which may be used on the vehicle. The dynamics associated with these systems will be added later as part of the ASE analysis. In addition, the aerodynamic modeling does not explicitly include circulation control blowing, although it is implicitly assumed that enough circulation control blowing is being used to maintain attached flow so that the aerodynamic theory used here is valid.

The equations of motion of a flexible, free-flying aircraft can be written in terms of vehicle rigid-body modes, vehicle structural vibration modes, and control surface deflection modes. For a finite number of modes n, the displacement of the vehicle is written as the product of mode shapes and time-dependent generalized coordinates as

$$d(t)=[\phi]^T\eta(t) \tag{1}$$

where d(t) is the vector of vehicle displacements at various points on the vehicle, $\eta(t)$ is an n vector of generalized coordinates, and the n columns of ϕ are the mode shapes of the vehicle.

Using this modal representation of the vehicle, the equations of motion are (Ref. 3)

$$[Ms^2 + Cs + K + qQ(s)]\xi + qQ_c(s)\delta = 0 \tag{2}$$

where s is the Laplace transform variable, ξ is the generalized coordinate vector of the rigid-body and vibration modes and δ is the vector of generalized coordinates for the control surface deflection modes such that $\eta^T = \{\xi^T\ \delta^T\}$, M, C, and K are the generalized mass, damping and stiffness matrices, respectively, and q is the dynamic pressure. The matrices Q(s) and $Q_c(s)$ are rational function approximations to tabulated unsteady generalized aerodynamic forces (GAF's) calculated for harmonic motion of the rigid-body, vibration, and control surface deflection modes. The approximation technique is described further below.

For this study, vehicle mode shape data representative of the RSRA/X-Wing configuration aircraft were obtained from Northrop Aircraft Corporation. These data were separated into symmetric and antisymmetric modes for the longitudinal and lateral model developments respectively. Table 1 lists the frequency and generalized masses of the rigid-body and elastic modes.

Unsteady GAF's as a function of reduced frequency $k = \omega b/V$, where ω is the frequency of oscillation, b is a reference length, and V is the velocity, were calculated for harmonic motion in ISAC using doublet lattice aerodynamics. The same aerodynamic paneling and structural interface was used for both the longitudinal and lateral cases. Figure 2 shows the aerodynamic panel layout and the location of the structural nodes for the X-Wing rotor alone. A surface-spline routine was used to calculate the displacements and slopes of each panel for every mode based on the mode shape data at the structural nodes. The panel displacements and slopes are used in doublet lattice to calculate the unsteady GAF's.

The GAF's calculated by doublet lattice are output as complex tabulated data as a function of the reduced frequency k for a given Mach number. These forces must be extended to arbitrary motion (complex frequency s) for use in dynamic stability analyses. The unsteady GAF's are modeled using a rational function approximation technique (Ref.s 4 and 5) as

$$[Q(s)\ |\ Q_c(s)] = A_0 + A_1\left(\frac{bs}{V}\right) + A_2\left(\frac{bs}{V}\right)^2 + \sum_{i=1}^{L}\frac{B_i s}{\left(s + \frac{V}{b}\beta_i\right)} \tag{3}$$

where the β_i are aerodynamic lag coefficients and L is the number of lags. The real matrices A_j and B_i are determined by a least-squares fit to the real and imaginary parts of the tabulated unsteady aerodynamic forces at $s = j\omega$ for a given set of lags β_i, which are arbitrarily selected to be within the reduced-frequency range of interest. For the longitudinal and lateral model developments four aerodynamic lags, $\beta_i = (0.1, 0.2, 0.35, 0.5)$, were used. In addition, constraints (Ref. 5) on the least-squares fits were applied to force exact agreement between the tabulated data and the approximations at k=0.

With the aerodynamic approximation of Eqn. 3 the equations of motion given by Eqn. 2 can be rewritten in state-space form as outlined in the Appendix. The resulting state-space model is then

$$\dot{x} = Fx + Gu \tag{4}$$

where x is the system state vector, F is the system dynamics matrix, G is the control input matrix, and u is the control input vector containing the control surface deflections δ, control surface rates, and control surface accelerations, as defined in the Appendix. The eigenvalues of the system matrix F, where F is a function of dynamic pressure q, are analyzed for system stability.

In order to validate the accuracy of the aerodynamic approximations and state-space models, a frequency response analysis of the open-loop aircraft was performed. Vertical displacement responses of right side forward-swept and aft-swept X-Wing blade tips to a sinusoidal oscillation of the lower horizontal tail (Fig. 1) were calculated using the state-space model. These results were compared with frequency response results obtained by substituting interpolated values of the tabulated GAF data directly into Eqn. 2 in place of the approximated aerodynamics and setting $s=j\omega$. Comparisons of the results in Figures 3 and 4 for both magnitude and phase show close agreement between results obtained with tabulated and approximated aerodynamics.

Dynamic Stability Analysis

The longitudinal and lateral dynamics state-space models of the flexible X-Wing aircraft in the stopped-rotor mode were analyzed for static and dynamic stability by computing system eigenvalues for a range of flight conditions, and plotting the results as a velocity root-locus. These analyses were performed to check for possible aeroelastic flutter, aeroelastic divergence, and possible body-freedom flutter, which is a coupling of rigid-body and flexible-body modes in an unstable flutter-like motion. The technique used leads to accurate estimates of instability speeds depending on the quality of the aerodynamic approximation in the reduced frequency range at which a mode crosses into the unstable right-half plane region.

Three series of analyses were performed, one each for the longitudinal and lateral dynamic models, and a third using a combined lateral/longitudinal model with a reduced set of symmetric and antisymmetric elastic vibration modes to check for possible coupling of the longitudinal and lateral dynamics. Two cases were run in both the lateral and longitudinal series, one using a model reduced to rigid-body modes only and the other using the complete set of rigid-body and elastic modes. The results of the third analysis series, which will not be shown, confirm that the longitudinal and lateral dynamics for the study configuration are uncoupled over the flight regime.

Lateral Stability - Eigenvalues of the system matrices of the rigid-body only and the full elastic model were computed for airspeeds from 50 to 300 knots at sea-level flight conditions using the ISAC computer code. The results are shown in the form of velocity root-loci in Figures 5 and 6. Figure 5 shows the full flexible model eigenvalue locations, with all the eigenvalues in the (stable) left-half plane over the velocity range, including a spiral mode eigenvalue near the origin, indicating that no aeroelastic antisymmetric flutter or divergence modes exist for this configuration. A comparison of the rigid-body analysis Dutch roll, spiral, and roll mode results with the full flexible model results for these modes are shown in Figure 6. The only significant difference due to flexibility of the vehicle is a slight loss of Dutch roll damping at the higher velocities.

Longitudinal Stability - An analysis of the longitudinal dynamics of the X-Wing aircraft similar to the lateral analysis described above was performed using both the rigid-body only and the full flexible models. For the same 50 to 300 knot velocity range at sea level as above, the locus of system eigenvalues of the flexible model are shown in Figure 7. These results show that the high frequency aeroelastic modes are all stable, however there is a single eigenvalue which moves along the real axis into the unstable right-half plane, passing through the origin at 230 knots. This unstable eigenvalue is shown more clearly in Figure 8, where the rigid-body only and flexible model short period mode dynamics are compared. As shown, the rigid-body only model exhibits a classical short period behavior with a complex conjugate eigenvalue pair increasing in frequency along a constant damping ratio line in the left-half plane. The flexible model results on the other hand show a different characteristic to the short period mode eigenvalues, with the initially complex conjugate pair quickly becoming two roots on the real axis, with one root moving to the left and the other to the right into the unstable right-half plane at 230 knots.

The short period root pattern of two real eigenvalues, although obviously due to the effects of structural flexibility in the present case, is characteristic of aircraft which are statically unstable. Therefore the predicted instability is due to structural deformations causing a loss of aircraft static margin. This loss of static margin is consistent with static aeroelastic 'washin' of the forward-swept blades (Ref. 6), which is the tendency of the load on the blade to increase the local section geometric angle-of-attack, causing a further increase in the aerodynamic load. Aeroelastic 'washin' of forward-swept wings leads to forward shifts in aerodynamic center locations and can ultimately lead to structural divergence of the wing. Similarly, aft-swept blades undergo static aeroelastic 'washout', which is the tendency of the load to result in a decrease in local section geometric angle-of-attack and thus limit the buildup of aerodynamic load due to deformation. Aeroelastic 'washout' of aft-swept wings also leads to forward shifts in aerodynamic center location. To verify that 'washin' and 'washout' were indeed the cause of the predicted instability, a static aeroelastic analysis method was formulated using a modal vibration approach to calculate static aeroelastic deformations and changes in

static stability derivatives. Those results are described in the next section.

Static Aeroelastic Analysis

The dynamic stability analyses described in the previous section were performed using first-order state-space mathematical models developed from the second-order matrix differential equations of motion of the vehicle, as given by Eqn. 2. For steady-state conditions, the tabulated GAF data for k=0 can be substituted directly into Eqn. 2 to obtain (Ref. 7)

$$[K + qQ(k=0)]\xi + qQ_c(k=0)\delta = 0 \qquad (5)$$

Partitioning Eqn. 5 according to rigid and flexible modes

$$\left[\begin{bmatrix} 0 & 0 \\ 0 & K_{ff} \end{bmatrix} + q\begin{bmatrix} Q_{rr} & Q_{rf} \\ Q_{fr} & Q_{ff} \end{bmatrix}\right]\begin{bmatrix} \xi_r \\ \xi_f \end{bmatrix} + q\begin{bmatrix} Q_{rc} \\ Q_{fc} \end{bmatrix}\delta = 0 \qquad (6)$$

gives two simultaneous equations in the two unknowns ξ_r and ξ_f, which are the rigid-body displacements and flexible-body modal-coordinate deflections, respectively. Solving the second of the two equations (second row of the matrix equation) for ξ_f in terms of ξ_r and δ,

$$\xi_f = (K_{ff} + qQ_{ff})^{-1}qQ_{fr}\xi_r + (K_{ff} + qQ_{ff})^{-1}qQ_{fc}\delta \qquad (7)$$

and substituting for ξ_f in the first equation (first row of the matrix equation) gives the result

$$[Q_{rr} + qQ_{rf}(K_{ff} + qQ_{ff})^{-1}Q_{fr}]\xi_r + [Q_{rc} + qQ_{rf}(K_{ff} + qQ_{ff})^{-1}Q_{fc}]\delta = 0 \qquad (8)$$

For combinations of rigid-body motion ξ_r and control-surface deflections δ the terms in Eqn. 8 contain the rigid-body aerodynamic forces (first term in square brackets) and the additional aerodynamic force due to static aeroelastic structural deformation (second term in square brackets). Dividing relevant elements of the total aerodynamic force matrix (square bracket term) due to rigid-body motion or control-surface deflection by the corresponding elements of the rigid-body only force matrix gives the ratio of flexible-body to rigid-body aerodynamic force as a function of dynamic pressure q. That is, the gain or loss of aerodynamic force due to structural deformation is given as a ratio, with a nearly rigid vehicle having flexible to rigid ratios near 1 for the entire q range of interest.

In the longitudinal direction, vertical translation z and pitch angle θ are the rigid-body mode displacements used in calculating unsteady GAF's and performing dynamic stability analyses. For steady-state, the aerodynamic force and moment due to z displacement are zero, meaning that the columns of Q_{rr} and Q_{fr} associated with z are zero. Thus, for example, the matrix Q_{rr} has the form

$$Q_{rr} = \begin{bmatrix} 0 & L_\theta \\ 0 & M_\theta \end{bmatrix} \qquad (9)$$

where L_θ is the lift due to pitch, and M_θ is the moment due to pitch. For small perturbations θ, these forces are the lift and moment due to angle-of-attack so that when the total aerodynamic force is divided by the rigid-body aerodynamic force, the results are flexible-to-rigid ratios of the aircraft lift-curve slope $C_{L\alpha}$ and the static-stability derivative $C_{M\alpha}$ since the dimensional quantities of dynamic pressure q, reference area S, and reference length c cancel out.

Flexible-to-rigid ratios of $C_{L\alpha}$ and $C_{M\alpha}$ for the trimmed X-Wing vehicle are shown in Figure 9 for airspeeds up to 300 knots at sea-level flight conditions. The effects of flexibility on lift-curve slope $C_{L\alpha}$ are slight and concentrated at the higher flight speeds, with a ratio of 1.14 or a 14% increase in lift at 300 knots. The effect on the static stability derivative $C_{M\alpha}$ is much more pronounced, with the flexible-to-rigid ratio decreasing rapidly with increasing airspeed, passing through zero at 230 knots and becoming of opposite sign, which corresponds directly to the passage of the real eigenvalue into the unstable region in Figures 7 and 8.

The nearly constant $C_{L\alpha}$ ratio and rapidly changing $C_{M\alpha}$ ratio imply a redistribution or shift in center of aircraft lift rather than a change in total aircraft lift. Dividing $C_{M\alpha}$ by $C_{L\alpha}$ at every airspeed gives the aerodynamic center location relative to the vehicle center of gravity (Ref. 8). This result is shown in Figure 10. The aerodynamic center at low airspeeds is aft of the center of gravity about 16 inches, generating nose-down stabilizing pitching moments for positive angle-of-attack disturbances. As the airspeed increases, the aerodynamic center moves forward toward the center of gravity, reducing the nose-down pitching moment and destabilizing the aircraft. Above 230 knots, the aerodynamic center is forward of the center of gravity generating unstable nose-up pitching moments due to positive angle-of-attack disturbances. This is the cause of the short period instability shown in Figure 8.

To investigate the 'washin' and 'washout' characteristics of the X-Wing blades in this study, structural deformations of a forward-swept and aft-swept blade were calculated for a one degree angle-of-attack change of the vehicle for a range of flight velocities at sea-level. Vertical blade displacements for this case are shown

in Figure 12. At the highest velocity, the forward-swept blade deflects upward at the tip about 1.7% of the blade length, which for this configuration is about a six inch actual vertical displacement. The aft-swept blade deflects slightly downward about 0.2% of the blade length at the tip, or about 0.7 inch actual displacement at that same dynamic pressure. This downward deflection is apparently due to downwash effects of the forward blade inducing a net negative angle-of-attack on the aft-swept blade, contributing even more to a forward shift in aerodynamic center than that due just to aeroelastic 'washout'. Note however that the doublet lattice aerodynamic theory used to predict these results assumes a flat, undeformed wake and therefore does not include the effects of deformations of the forward-swept blade wake on the aft-swept blade aerodynamics. These effects could be substantial, and could either alleviate or further aggravate the shifts in aerodynamic center locations.

Plots of the local section geometrical angle-of-attack changes due only to vertical-bending deflection of the blades for the one degree aircraft angle-of-attack condition are shown in Figure 13. The forward-swept blade shows increasing angles-of-attack due to vertical deflections ('washin'), with a six degree increase at the tip for the highest dynamic pressure. For the aft-swept blade, the downward deflection results in an increase in local section geometrical angle-of-attack along the span. This has the effect of reducing the down lift being generated on the aft blade by downwash from the forward blade, thereby unloading the outboard sections of the aft blade.

Changes in blade lift distributions due to static structural deformation as a function of flight speed are shown in Figures 14 and 15. Figure 14 shows an increasing load distribution with increased velocity as well as an outboard (forward) shift in the center of the lift distribution. Figure 15 shows a reduction in outboard lift as velocity increases, corresponding to the aeroelastic 'washout' of the aft-swept blade. At 300 knots, the outboard third of the blade is actually carrying a down load and the center-of-lift has shifted substantially inboard (forward).

Static aeroelastic deformations of stopped X-Wing rotor system blades changing aircraft static margins and longitudinal stability and trim characteristics will likely be a generic problem for X-Wing configuration aircraft. In the stopped-rotor mode, several of the X-Wing rotor blades will have to be in a forward-swept position and will undergo aeroelastic 'washin' deformations. Furthermore, aeroelastic structural tailoring of composite structural material to force aeroelastic 'washout' of the forward-swept wing (Ref. 9) will probably not be possible on X-Wing rotor blades because of the requirements of rotary-wing flight and conversion from rotary-wing to fixed-wing flight modes. Control of the static aeroelastic blade deformations may well require the use of outboard control surfaces on the rotor blades or additional circulation control blowing to varying degrees along the blade.

Conclusions

A static and dynamic aeroelastic stability analysis of an X-Wing configuration aircraft including the aircraft flight dynamics (free-body) modes has been conducted. Lateral directional analysis results using antisymmetric aircraft vibration modes showed only a slight decrease in Dutch roll mode damping due to X-Wing blade flexibility effects. Longitudinal analysis results using symmetric vibration modes showed a dramatic change in aircraft short period eigenvalues due to structural flexibility, leading to an unstable root pattern and a statically unstable aircraft.

A static aeroelastic analysis using a normal vibration mode approach was used to determine flexible-to-rigid ratios of the study configuration aircraft lift-curve slope, static stability derivative (moment-curve slope), and aerodynamic-center location relative to the aircraft center of gravity. These results showed that the aircraft aerodynamic center shifted forward with increasing speed, leading to the previously mentioned static instability. Analysis of the blade deformations showed that aeroelastic 'washin' of the forward-swept blades combined with downwash induced down load on the aft-swept blade caused the aerodynamic center shift. Reductions in aircraft static margin and aircraft trim changes due to structural deformation are likely to be generic problems of X-Wing configuration aircraft and may require active blade deformation control for X-Wing aircraft to achieve stable high speed forward flight.

Appendix

Transformation of Eqn.s 2 and 3 into state-space form along the lines of Ref. 3 is accomplished as follows. The matrices A_j and B_i in Eqn. 3 are partitioned as

$$A_j = [A_j^{\xi} \mid A_j^{c}] \tag{A1.a}$$

$$B_i = [B_i^{\xi} \mid B_i^{c}] \tag{A1.b}$$

and the resulting expression for Eqn. 3 is substituted into Eqn. 2 to get

$$[Ms^2 + Cs + K + \sum_{i=1}^{L} w_i^{\xi} s]\xi + [qA_0^{c} + qA_1^{c}\left(\frac{bs}{V}\right) + qA_2^{c}\left(\frac{bs}{V}\right)^2 + \sum_{i=1}^{L} w_i^{c} s]\delta = 0 \tag{A2}$$

where

$$M = M + qA_2^{\xi}\frac{b^2}{V^2}$$

$$C = C + qA_1^{\xi}\frac{b}{V}$$

$$K = K + qA_0^{\xi}$$

$$w_i^{\xi} = \frac{qB_i^{\xi}}{s + \frac{V}{b}\beta_i}$$

$$w_i^{c} = \frac{qB_i^{c}}{s + \frac{V}{b}\beta_i}$$

Defining a vector x_i^a as

$$x_i^a = w_i^{\xi} s\xi + w_i^{c} s\delta$$
$$= \frac{qs}{s + \frac{V}{b}\beta_i}[B_i^{\xi}\xi + B_i^{c}\delta] \qquad (A3)$$

and expanding gives

$$sx_i^a = -\beta_i\frac{V}{b}Ix_i^a + qsB_i^{\xi}\xi + qsB_i^{c}\delta \qquad (A4)$$

which is a first-order equation for the aerodynamic lags associated with the unsteady GAF's. Defining a system state vector x and control input vector u as

$$x^T = \{\xi^T\ s\xi^T\ x_1^{a^T} \ldots x_L^{a^T}\} \qquad (A5)$$

and

$$u^T = \{\delta^T\ s\delta^T\ s^2\delta^T\} \qquad (A6)$$

Eqn.s A2 and A4 can be combined as

$$sx = Fx + Gu \qquad (A7)$$

or in the time domain

$$\dot{x} = Fx + Gu \qquad (A8)$$

where the matrices F and G are

$$F = \begin{bmatrix} 0 & I & 0 & \ldots & 0 \\ -M^{-1}K & -M^{-1}C & -M^{-1} & \ldots & -M^{-1} \\ 0 & qB_1^{\xi} & -\beta_1\frac{V}{b}I & 0 & \ldots \\ : & : & 0 & . & \ldots \\ 0 & qB_L^{\xi} & : & \ldots & -\beta_L\frac{V}{b}I \end{bmatrix}$$

$$G = q\begin{bmatrix} 0 & 0 & 0 \\ -M^{-1}A_0^{c} & -M^{-1}A_1^{c}\frac{b}{V} & -M^{-1}A_2^{c}\frac{b^2}{V^2} \\ 0 & B_1^{c} & 0 \\ : & : & : \\ 0 & B_L^{c} & 0 \end{bmatrix}$$

which is the same as Eqn. 4 in the paper.

References

1. Lambert, M. 'X-Wing Harrier Speed and Helicopter Hovering', Interavia Review, No. 5/1985.

2. Peele, E. L., and Adams, W. M. Jr., 'A Digital Program for Calculating the Interaction Between Flexible Structures, Unsteady Aerodynamics, and Active Controls', NASA TM 80040, Jan. 1979.

3. Mukhopadhyay, V., Newsom, J. R., and Abel, I., 'A Method for Obtaining Reduced-Order Control Laws for High-Order Systems Using Optimization Techniques', NASA TP 1876, August 1981.

4. Tiffany, S. H., and Adams, W. M. Jr., 'Fitting Aerodynamic Forces in the Laplace Domain: An Application of a Nonlinear Nongradient Technique to Multilevel Constrained Optimization', NASA TM 86317, October 1984.

5. Abel, I. 'An Analytical Technique for Predicting the Characteristics of a Flexible Wing Equipped With an Active Flutter-Suppression System and Comparison With Wind-Tunnel Data', NASA TP 1367, 1979.

6. Bisplinghoff, R. L., Ashley, H., and Halfman, R. L., *Aeroelasticity*, Addison-Wesley Publishing Co., 1955.

7. Sheena, Z., and Karpel, M., 'Static Aeroelastic Analysis Using Aircraft Vibration Modes', Second International Symposium on Aeroelasticity and Structural Dynamics, Aachen W. Germany, April 1985, pg. 229-232.

8. Abel, I., 'A Wind-Tunnel Evaluation of Analytical Techniques for Predicting Static Stability and Control Characteristics of Flexible Aircraft', NASA TN D-6656, March 1972.

9. Weisshaar, T. A., 'Aeroelastic Tailoring of Forward Swept Composite Wings', Journal of Aircraft, Vol. 18, No. 8, August 1981, pg.669-676.

Table 1. Vehicle Modal Data

Symmetric		Antisymmetric	
Freq. (Hz.)	Mass (lb-sec^2/in)	Freq. (Hz.)	Mass (lb-sec^2/in)
0.0	86.84	0.0	86.15
0.0	4.85	0.0	7.14
3.64	1.29	0.0	5.72
5.09	0.71	1.79	2.03
5.61	2.01	4.44	1.36
6.58	1.31	4.91	1.24
8.91	0.50	5.08	0.79
8.99	2.39	6.07	0.35
10.5	1.75	6.19	0.88
12.2	1.62	6.25	0.88
13.2	1.93	6.32	10.8
14.5	0.013	6.54	1.19
16.5	0.006	6.63	1.35
17.7	0.033	6.76	12.4
20.3	0.014	7.50	0.84
20.9	0.112	7.57	0.82
22.0	0.80	8.53	8.94
24.2	1.00	9.85	1.19
26.4	0.141	10.8	0.54
29.4	0.129	12.0	1.25

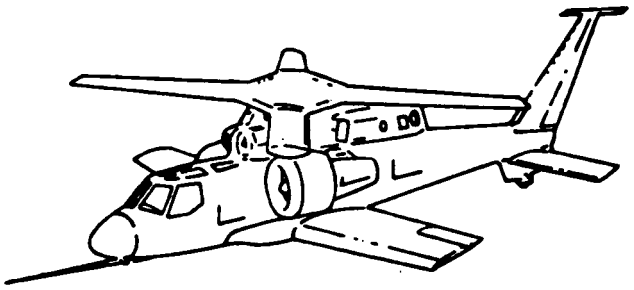

Fig. 1 The RSRA/X-Wing vehicle

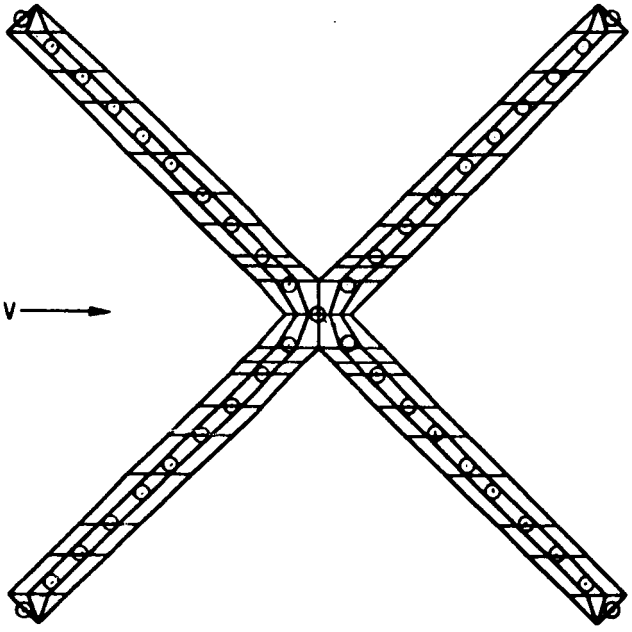

Fig. 2 X-Wing rotor aerodynamic paneling and structural node locations

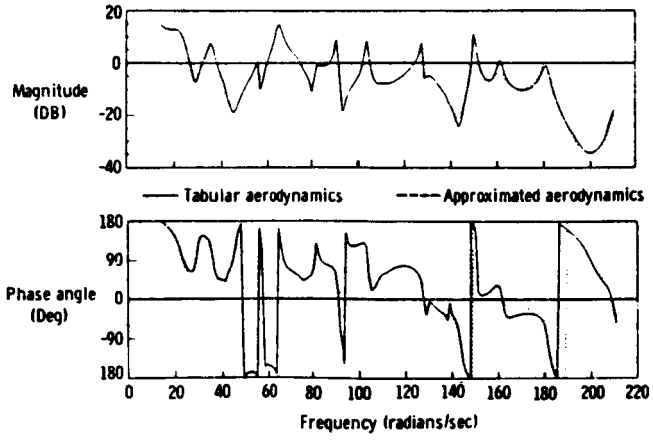

Fig. 3 Right side forward blade tip displacement response to lower horizontal stabilizer input (V=200 kts, sea level)

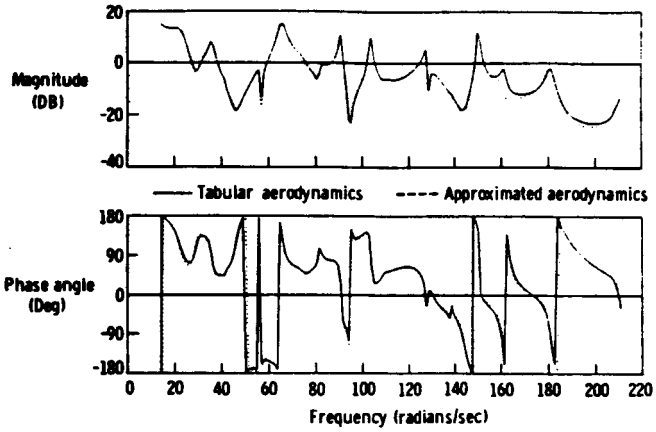

Fig. 4 Right side aft blade tip displacement response to lower horizontal stabilizer input (V=200 kts, sea level)

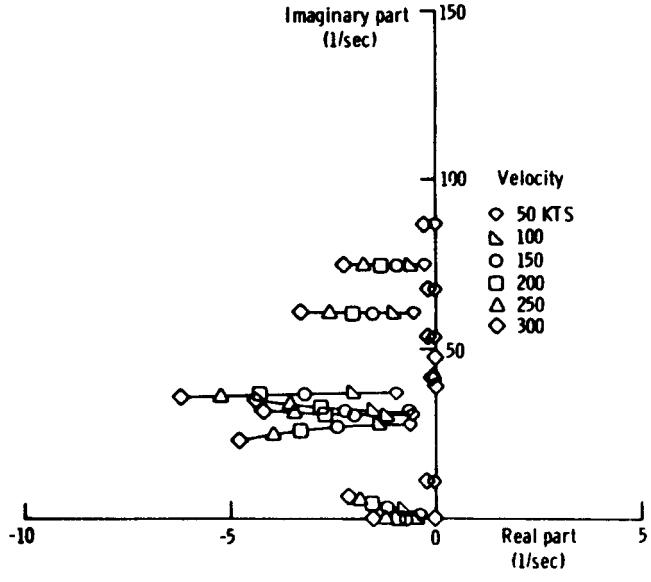

Fig. 5 Eigenvalue velocity root locus for lateral motion of flexible model at sea level

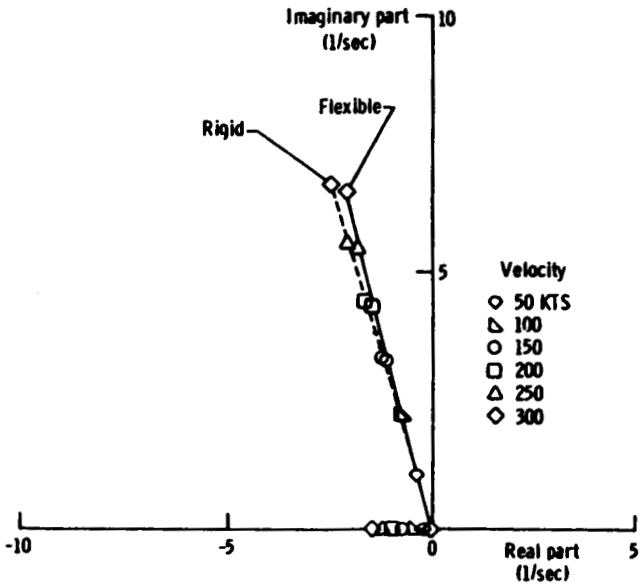

Fig. 6 Comparison of lateral-directional velocity root loci for rigid and flexible models at sea level

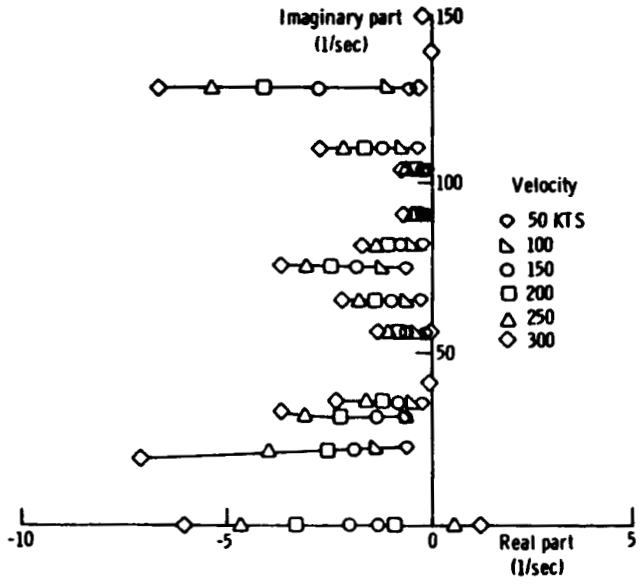

Fig. 7 Eigenvalue velocity root locus for longitudinal motion of flexible model at sea level

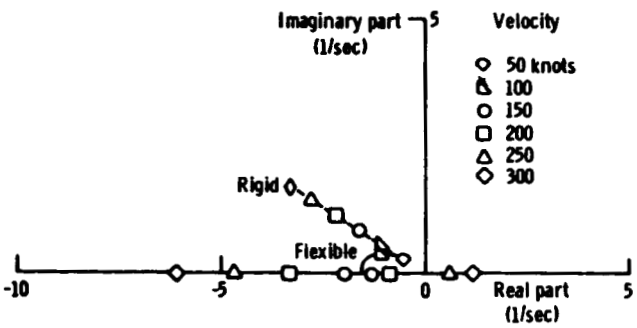

Fig. 8 Comparison of longitudinal velocity root loci for rigid and flexible models at sea level

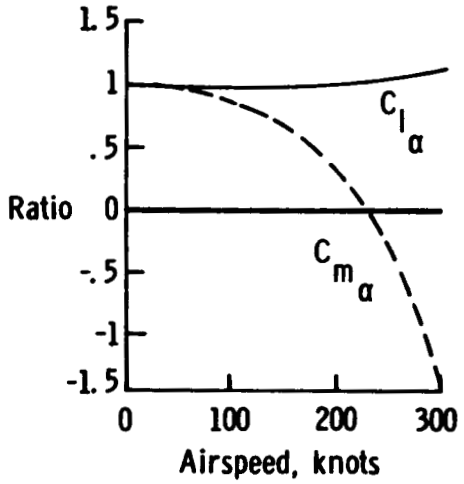

Fig. 9 Flexible-to-rigid ratios of $C_{L\alpha}$ and $C_{M\alpha}$ at sea level

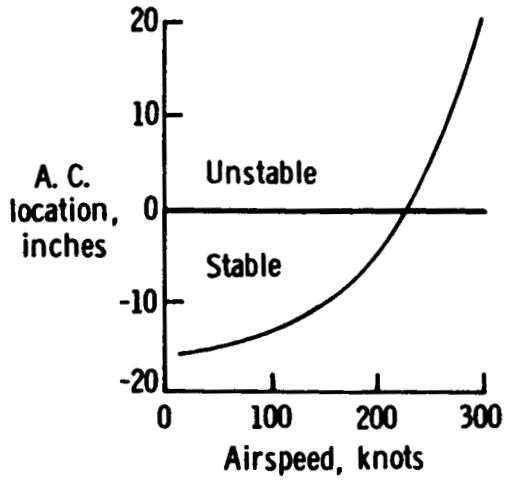

Fig. 10 Vehicle aerodynamic-center location relative to center of gravity at sea level

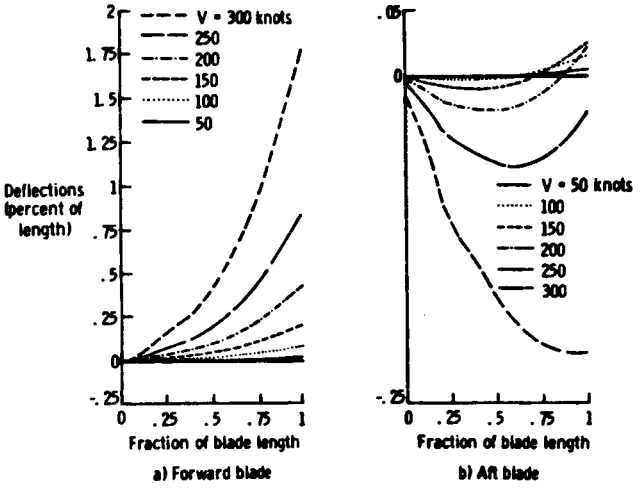

Fig. 11 Vertical static aeroelastic deflections of blades at sea level

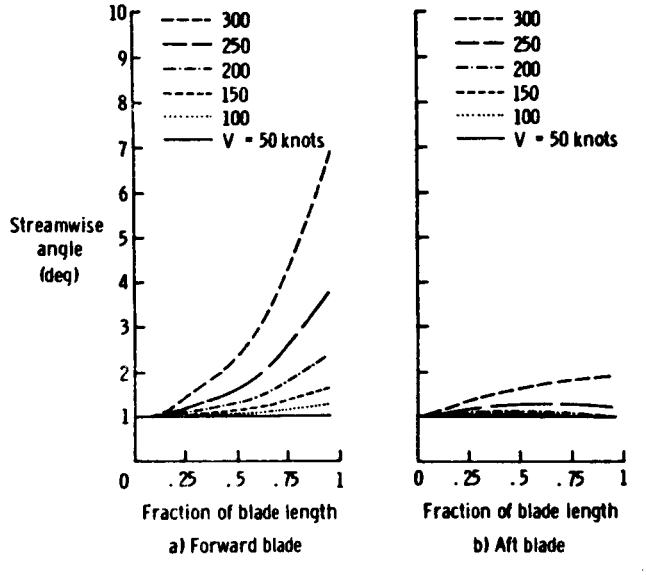

Fig. 12 Local section geometric angles of attack due to vertical blade deflection

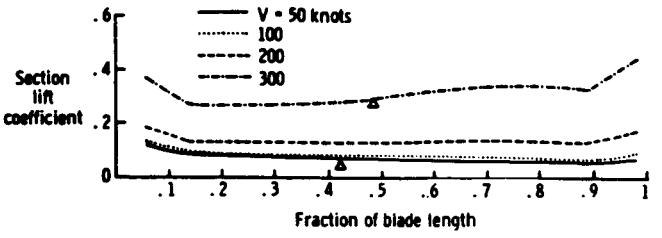

Fig. 13 Forward-blade lift distribution and center location at sea level

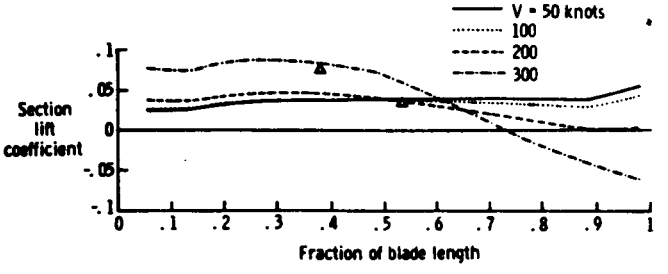

Fig. 14 Aft-blade lift distribution and center location at sea level

1. Report No.	2. Government Accession No.	3. Recipient's Catalog No.
NASA TM-100480		

4. Title and Subtitle	5. Report Date
The Effects of Aeroelastic Deformation on the Unaugmented Stopped-Rotor Dynamics of an X-Wing Aircraft	June 1987
	6. Performing Organization Code
7. Author(s)	8. Performing Organization Report No.
Michael G. Gilbert and Walter A. Silva	
9. Performing Organization Name and Address	10. Work Unit No.
NASA Langley Research Center Hampton, VA 23665-5225	532-98-91-51
	11. Contract or Grant No.
12. Sponsoring Agency Name and Address	13. Type of Report and Period Covered
National Aeronautics and Space Administration Washington, DC 20546-0001	Technical Memorandum
	14. Sponsoring Agency Code

15. Supplementary Notes Michael G. Gilbert, Aerospace Engineer, Aeroservoelasticity Branch, Loads and Aeroelasticity Division, NASA Langley Research Center, Hampton, VA. Walter A. Silva, Structures Engineer, PRC-Kentron, Inc., Hampton, VA. Presented at AIAA Atmospheric Flight Mechanics Conference, Monterey, CA, on August 19, 1987.

16. Abstract

A new design concept in the development of vertical takeoff and landing aircraft with high forward flight speed capability is that of the X-Wing. The X-Wing is a stiff, bearingless helicopter rotor system which can be stopped in flight and the blades used as two forward-swept wings and two aft-swept wings. Because of the unusual configuration in the fixed-wing mode, there is a high potential for aeroelastic divergence or flutter and coupling of blade vibration modes with rigid-body modes. An aeroelastic stability analysis of an X-Wing configuration aircraft was undertaken to determine if these problems could exist. This paper reports on the results of dynamic stability analyses in the lateral and longitudinal directions including the vehicle rigid-body and flexible modes. A static aeroelastic analysis using the normal vibration mode equations of motion was performed to determine the cause of a loss of longitudinal static margin with increasing airspeed. This loss of static margin was found to be due to aeroelastic 'washin' of the forward-swept blades and 'washout' of the aft-swept blades moving the aircraft aerodynamic center forward of the center of gravity. This phenomenon is likely to be generic to X-Wing aircraft.

17. Key Words (Suggested by Author(s))	18. Distribution Statement
X-Wing/stability/aeroelastics flight dynamics	Unclassified - Unlimited Subject Category 39

19. Security Classif. (of this report)	20. Security Classif. (of this page)	21. No. of Pages	22. Price
Unclassified	Unclassified	11	A02

For sale by the National Technical Information Service, Springfield, Virginia 22161